Implementation of sine condition test to measure optical system misalignments

Sara Lampen,* Matthew Dubin, and James H. Burge

College of Optical Sciences, University of Arizona, Tucson, Arizona 85721, USA

*Corresponding author: sara.m.lampen@gmail.com

Received 19 August 2011; revised 17 October 2011; accepted 24 October 2011;
posted 24 October 2011 (Doc. ID 153147); published 25 November 2011

Rather than measuring aberrations across the field to quantify the alignment of an optical system, we show how a single, on-axis measurement of the pupil mapping can be used to measure the off-axis performance of the system and determine the state of alignment. In this paper we show how the Abbe sine condition can be used to relate the mapping between the entrance and exit pupils to image aberrations that have linear field dependence. This mapping error then can be used to measure the linear astigmatism caused by the misalignment. Additionally, we present experimental results from the sine condition test on a simple system. © 2011 Optical Society of America

OCIS codes: 220.1010, 220.1140, 220.4840.

1. Introduction

Originally proposed in 1873 by Abbe [1], the sine condition has long been used as a tool for designing optical systems. When the sine condition is employed on a system that is well corrected on-axis, the system can be designed such that it has coma-free imaging for small fields [2,3]. Abbe called such a system "aplanatic" [4]. Since Abbe first introduced the concept, there have been several expansions of the sine condition. For example, Shibuya [5] derives the exact sine condition in the presence of spherical aberration, and Zhao and Burge [6] have developed additional conditions that allow for the correction of quadratic-field-dependent aberrations in addition to the correction of the linearly field dependent aberrations provided by the sine condition.

The purpose of this paper is to expand on the idea originally proposed by Burge *et al.* [7] that the sine condition can be used to control linearly field-dependent aberrations that are due to misalignment. Other methods that use measurements at several field points to align optical systems have been proposed. For example, the collimation method first proposed by McLeod [8], and then expanded on by Noethe [9] and Lee [10], measures the field at different points and derives the misalignments of the optical elements. Additionally, Tessieres used measurements at several field points to determine the state of alignment [11].

One of the advantages of the sine condition test (SCTest) over other tests is that all of the test equipment can be aligned to the center of the field while making measurements of the off-axis performance, which reduces the uncertainty of the measurement. The uncertainty is further reduced in systems with coma by using the test equipment to counteract the coma. In this paper, we will show how the sine condition can be used to align optical systems by providing a brief explanation of the sine condition and then giving a description of how the measurements of the pupil mapping can be made. The pupil mapping is then used to measure the linear astigmatism to quantify the effects of the misalignments, which include both tilts and decenters of the optical elements. Last, we will show experimental results taken with this measurement concept on a simple system.

2. Sine Condition Derivation

A number of other sources have provided explanations and derivations of the sine condition [12–15].

0003-6935/11/346391-08$15.00/0

For this paper we will provide a general derivation of the sine condition that emphasizes how it can be used to find the mapping between the entrance (EP) and exit pupils (XP). This pupil mapping can then be used to evaluate the system alignment.

Figure 1(a) shows the geometry of the optical system for this derivation. The object point O is the reference point for the measurement with its conjugate point I in image space. It is assumed that there is low wavefront error at O and I. Point B is a point on the EP located at $(x_{\mathrm{EP}}, y_{\mathrm{EP}})$ that is imaged onto the XP at point C at $(x_{\mathrm{XP}}, y_{\mathrm{XP}})$. It is assumed that all of the rays that enter the EP at B will exit the XP at C and the EP and XP are at the paraxial image locations of the aperture stop. Additionally, ε_o is an off-axis object point a small distance from O with a conjugate point ε_i.

The wavefront phase difference at the EP, $W_o(x_{\mathrm{EP}}, y_{\mathrm{EP}})$, is the difference between the on-axis point O and the off-axis point ε_o, which is the scalar path difference between those two points:

$$W_o(x_{\mathrm{EP}}, y_{\mathrm{EP}}) = \overline{OB}(x_{\mathrm{EP}}, y_{\mathrm{EP}}) - \overline{\varepsilon_o B}(x_{\mathrm{EP}}, y_{\mathrm{EP}}) = \Delta D(x_{\mathrm{EP}}, y_{\mathrm{EP}}). \quad (1)$$

This difference ΔD is shown in Fig. 1(b), where ε_o is small with respect to the distance to the EP, such that $\Delta D \approx \Delta d$. Equation (1) then reduces to

$$W_o(x_{\mathrm{EP}}, y_{\mathrm{EP}}) \approx \Delta d = \hat{\mathbf{S}}_\mathbf{o} \bullet \boldsymbol{\varepsilon}_\mathbf{o} = \varepsilon_{o,x} \frac{x_{\mathrm{EP}}}{R_o} + \varepsilon_{o,y} \frac{y_{\mathrm{EP}}}{R_o}, \quad (2)$$

where $\boldsymbol{\varepsilon}_\boldsymbol{o}$ is the vector from point O to point ε_o. The unit vector $\hat{\mathbf{S}}_\mathbf{o}$ can be expressed in terms of the direction cosines. In this derivation it is useful to express $\hat{\mathbf{S}}_\mathbf{o}$ both as $(x_{\mathrm{EP}}/R_O, y_{\mathrm{EP}}/R_O)$, where R_o is the object wavefront radius of curvature at the EP from ε_o, and later as $(|\hat{\mathbf{S}}_{\mathbf{o},\mathbf{x}}| \sin\theta_{o,x}, |\hat{\mathbf{S}}_{\mathbf{o},\mathbf{y}}| \sin\theta_{o,y})$.

We then define the mapping between the coordinates $(x_{\mathrm{EP}}, y_{\mathrm{EP}})$ in the EP and $(x_{\mathrm{XP}}, y_{\mathrm{XP}})$ in the XP as

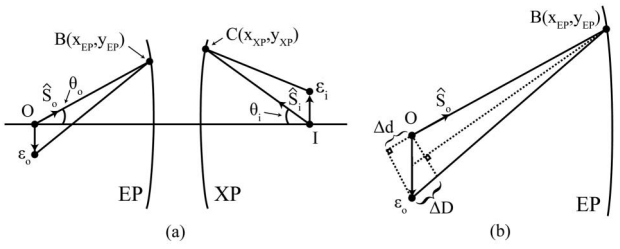

Fig. 1. (a) General illustration of an axisymmetric optical system with finite conjugates: O, object point; I, conjugate image point; B, point on entrance pupil (EP); C, point on exit pupil (XP) conjugate to B; ε_o, off-axis object point; ε_i, conjugate off-axis image point; $\hat{\mathbf{S}}_\mathbf{o}$, unit vector pointing from O to B; θ_o, angle of $\hat{\mathbf{S}}_\mathbf{o}$ with respect to the axis; $\hat{\mathbf{S}}_\mathbf{i}$, unit vector from I to C; θ_i, angle of $\hat{\mathbf{S}}_\mathbf{i}$ with respect to the axis. (b) Close-up of object space: ΔD, exact scalar path difference between O and ε_o; Δd, approximate scalar path difference.

$$x_{\mathrm{EP}} = m_x x_{\mathrm{XP}} + f_x(x_{\mathrm{XP}}, y_{\mathrm{XP}}),$$
$$y_{\mathrm{EP}} = m_y y_{\mathrm{XP}} + f_y(x_{\mathrm{XP}}, y_{\mathrm{XP}}), \quad (3)$$

where $f_x(x_{\mathrm{XP}}, y_{\mathrm{XP}})$ is the x component of the functional form of the pupil mapping error at the XP coordinate $(x_{\mathrm{XP}}, y_{\mathrm{XP}})$, and $f_y(x_{\mathrm{XP}}, y_{\mathrm{XP}})$ is the y component. While the exact point-to-point mapping from the EP and the XP is determined by the optical system, through Fermat's principle we know that the optical path length between a given point $(x_{\mathrm{EP}}, y_{\mathrm{EP}})$ on the EP to its conjugate point $(x_{\mathrm{XP}}, y_{\mathrm{XP}})$ on the XP is stationary, and therefore the wavefront phase difference is constant. Thus, $W_o(x_{\mathrm{EP}}, y_{\mathrm{EP}}) = W_I(x_{\mathrm{XP}}, y_{\mathrm{XP}})$, and Eq. (3) can be substituted into Eq. (2), yielding

$$W_o(x_{\mathrm{EP}}, y_{\mathrm{EP}}) = W_I(x_{\mathrm{XP}}, y_{\mathrm{XP}}),$$
$$\varepsilon_{o,x} \frac{x_{\mathrm{EP}}}{R_o} + \varepsilon_{o,y} \frac{y_{\mathrm{EP}}}{R_o} = \frac{\varepsilon_{o,x}}{R_o} [m_x x_{\mathrm{XP}} + f_x(x_{\mathrm{XP}}, y_{\mathrm{XP}})] + \frac{\varepsilon_{o,y}}{R_o} [m_y y_{\mathrm{XP}} + f_y(x_{\mathrm{XP}}, y_{\mathrm{XP}})]. \quad (4)$$

Next, the magnification between ε_o and ε_i, as well as the magnification between the object wavefront radius of curvature and the image wavefront radius of curvature are used to rewrite Eq. (4) as

$$\varepsilon_{o,x} \frac{x_{\mathrm{EP}}}{R_o} + \varepsilon_{o,y} \frac{y_{\mathrm{EP}}}{R_o} = \frac{1}{m} \left[\varepsilon_{i,x} \frac{x_{\mathrm{XP}}}{R_i} + \varepsilon_{i,y} \frac{y_{\mathrm{XP}}}{R_i} \right] + \frac{1}{R_o} [\varepsilon_{o,x} f_x(x_{\mathrm{XP}}, y_{\mathrm{XP}}) + \varepsilon_{o,y} f_y(x_{\mathrm{XP}}, y_{\mathrm{XP}})]. \quad (5)$$

In Eq. (5), terms one and two are the ideal object and ideal wavefront phase difference and term three is the pupil mapping error, W_{PME}. Remembering that

$$\frac{x_{\mathrm{EP}}}{R_o} = |\hat{\mathbf{S}}_{\mathbf{o},\mathbf{x}}| \sin\theta_{o,x}, \qquad \frac{y_{\mathrm{EP}}}{R_o} = |\hat{\mathbf{S}}_{\mathbf{o},\mathbf{y}}| \sin\theta_{o,y}, \quad (6)$$

and solving for W_{PME}, Eq. (5) can be rewritten as

$$W_{\mathrm{PME}} = (\varepsilon_{o,x} \sin\theta_{o,x} + \varepsilon_{o,y} \sin\theta_{o,y}) - \frac{1}{m} (\varepsilon_{i,x} \sin\theta_{i,x} + \varepsilon_{i,y} \sin\theta_{i,y}). \quad (7)$$

This can be stated directly in vector form as

$$W_{\mathrm{PME}} = \hat{\mathbf{S}}_\mathbf{o} \bullet \boldsymbol{\varepsilon}_\mathbf{o} - \frac{1}{m} \hat{\mathbf{S}}_\mathbf{i} \bullet \boldsymbol{\varepsilon}_\mathbf{i}. \quad (8)$$

It is easy to see that when there is no pupil mapping error, Eq. (7) reduces to the classic form of the sine condition. To help visualize the pupil mapping error, Fig. 2 shows how to use Eq. (8). The pupil mapping error shown in Step 1 is for an axisymmetric system that has coma, where the tail of the arrow is the location on the XP where a ray would have exited had the sine condition been strictly satisfied. The head of the

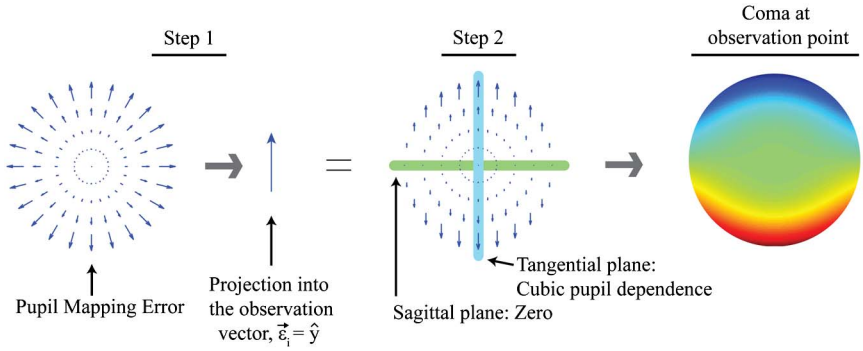

Fig. 2. (Color online) Illustration of how the pupil mapping error found using Eq. (8) can be used to find the linearly field dependent aberrations of an optical system.

arrow is the true location of the ray. In order to find the linearly field-dependent aberrations present, the projection of the pupil mapping onto the observation vector, ε_i, is found. In this example $\varepsilon_i = \hat{y}$. This projection is represented in the quiver plot shown in Step 2, which has a cubic dependency in the tangential plane and a value of zero in the sagittal plane. When this is fitted with Zernike polynomials, the result is the amount of coma at the field point associated with the observation vector.

In general, coma can be written as

$$W_{\text{Coma}} = C(H_x Z_8 + H_y Z_7), \tag{9}$$

where C is a constant, H_x and H_y are the x and y field positions, Z_7 is 90° coma, and Z_8 is 0° coma [see Eq. (10)]:

$$Z_7 = (3\rho^3 - 2\rho)\sin\theta, \qquad Z_8 = (3\rho^3 - 2\rho)\cos\theta. \tag{10}$$

Figure 3 shows the field and pupil dependencies of coma. The top row of the figure emphasizes the linear dependence of the coma when H_y and then H_x are set to zero, as well as the general field dependence of W_{Coma}. The bottom row shows the pupil dependence for Z_7 and Z_8.

Additionally, it was assumed earlier that all of the rays that entered the EP at a specific point B would exit at a conjugate point C [see Fig. 1], which places a practical restraint on the size of ε_o. As a result, the pupil mapping error found through Eq. (8) is only sensitive to aberrations that have linear field dependence. Because of this, in the perfectly aligned, axisymmetric system the SCTest would only be sensitive to coma. However, when a system is misaligned, the field dependence of the astigmatism of the system gains a linear component in addition to the native quadratic field dependence [7,8,16]. For simplicity, linearly field dependent astigmatism will be referred to as linear astigmatism. By relating the pupil distortion to this linear astigmatism, the alignment of the optical system can be measured using the SCTest.

3. Linear Astigmatism Explanation

Linear astigmatism was first discussed by Shack and Thompson [16] as the linear component of binodal astigmatism, which exists when linear astigmatism from misalignments, such as tilt and decenter, combines with the native quadratic field astigmatism. Because the SCTest is only sensitive to the linearly field-dependent aberrations, we will limit our discussion to linear astigmatism. Note, for an axisymmetric system, linear astigmatism is only present when there is an error in the optical system, so it is a useful indicator of the state of alignment. The general form of linear astigmatism, W_{LA}, can be defined in terms of Zernike standard polynomials [see Eq. (11)]:

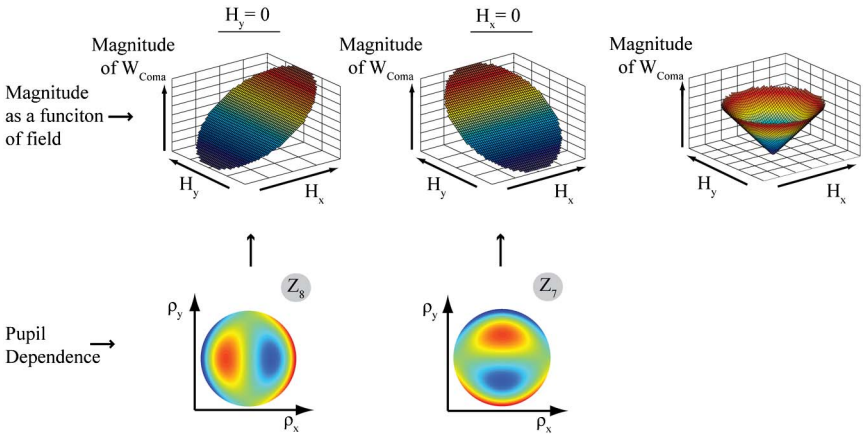

Fig. 3. (Color online) Field dependence of W_{Coma} (top row) and pupil dependence of W_{Coma} (bottom row).

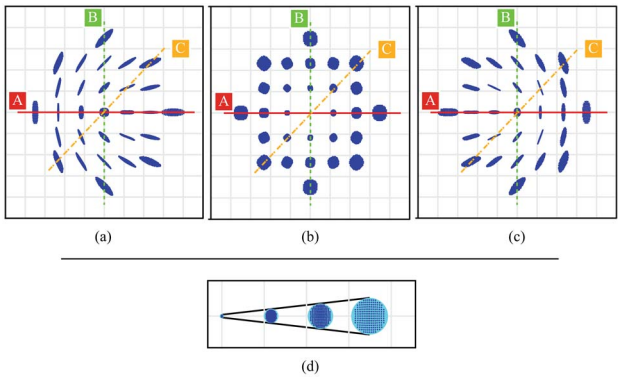

Fig. 4. (Color online) (a)–(c) Full field spot diagrams of linear astigmatism shown through focus, plots without annotations originally seen in [7]. (d) Close-up of the spots from plot (b) to show the linear nature of the field dependence.

$$W_{\mathrm{LA}} = C(H_x Z_6 + H_y Z_5), \tag{11}$$

where C is a constant, H_x and H_y are the field positions in the x and y directions, Z_5 is 45° astigmatism, and Z_6 is 0° astigmatism [see Eq. (12)]. There is also a linear focus term that appears along with linear astigmatism, which is simply a focal plane tilt:

$$Z_5 = \rho^2 \sin 2\theta, \qquad Z_6 = \rho^2 \cos 2\theta. \tag{12}$$

Figure 4 shows the full field spot diagrams of linear astigmatism to help illustrate how Eq. (11) varies across the field and through focus. This type of plot for linear astigmatism is sometimes called "dreamcatcher" astigmatism [17]. Along solid line A, where H_x varies and $H_y = 0$, W_{LA} only consists of 0° astigmatism and linear focus. Along line B, W_{LA} is only dependent on H_y in the field, and so it only consists of 45° astigmatism. As the field progresses from line A to line B, W_{LA} is the superposition of 0° and 45° astigmatism, so that along line C, W_{LA} is an equal mix of the two forms of astigmatism. These dependences along cross sections A, B, and C are the same for plots (a)–(c). Also, as the plots move through focus from plot (a)–(c), the orientation of the spots for a given field rotates 90°. To emphasize that W_{LA} has a linear field dependence, Fig. 4(d) shows a close-up of the spots from Fig. 4(b) as the field increases, where the black line shows how the size of the spots linearly increases.

Figure 5 shows the field and pupil dependence of linear astigmatism, similar to Fig. 3. It can be seen from these two figures that while the pupil dependence of coma and linear astigmatism differ, both have a linear field dependence that the SCTest is sensitive to.

Tying linear astigmatism back to the pupil mapping provided by the SCTest, Fig. 6 shows the form of the pupil mapping error created by linear astigmatism. Similar to Fig. 2, Fig. 6 shows how to use Eq. (8). When the pupil mapping error in Step 1 is projected onto the observation vector, $\varepsilon_{\mathbf{i}} = \hat{\mathbf{x}}$, the complicated form of the pupil mapping reduces to the simpler quiver plot representation shown in Step 2. When fitted with Zernike polynomials, the result is the amount of 0° astigmatism at the field point associated with observation vector. Conversely, when the pupil mapping is projected onto $\varepsilon_{\mathbf{i}} = \hat{\mathbf{y}}$, the result is represented by the quiver plot in Step 2, and when fitted with Zernike polynomials, the result is the amount of 45° astigmatism.

When the linear astigmatism shown in Fig. 4 is added to the native quadratic astigmatism, the result is binodal astigmatism. A number of methods exist to use binodal astigmatism as a way to quantify the misalignment of a system [18]. In systems that have little coma, binodal astigmatism can be measured relatively easily because there are no other linearly field-dependent aberrations to hinder the measurement of the linear component of the astigmatism. On the other hand, in systems with coma, it is difficult to measure the linear field dependence of the astigmatism on top of the coma with low uncertainty [16]. However, as will be seen in Section 5, the components of the SCTest can be used to mask the coma and provide a low uncertainty measurement of the system misalignment.

4. General Measurement

The first step in the SCTest is to use the sine condition to find the mapping between the entrance and

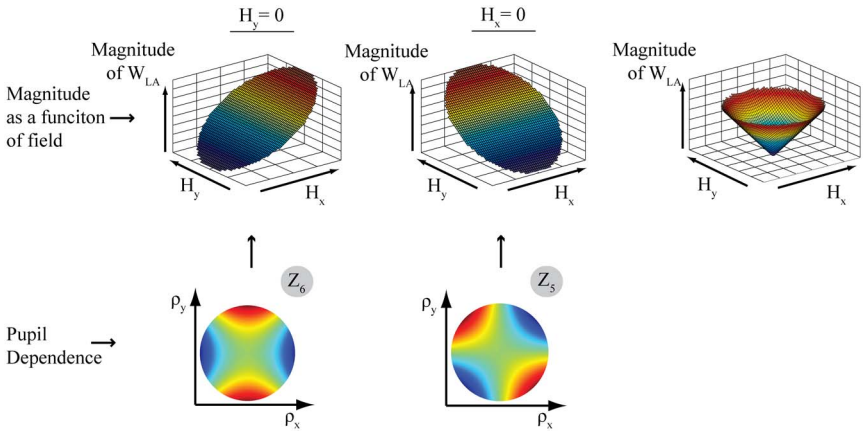

Fig. 5. (Color online) Field dependence of W_{LA} (top row) and pupil dependence of W_{LA} (bottom row).

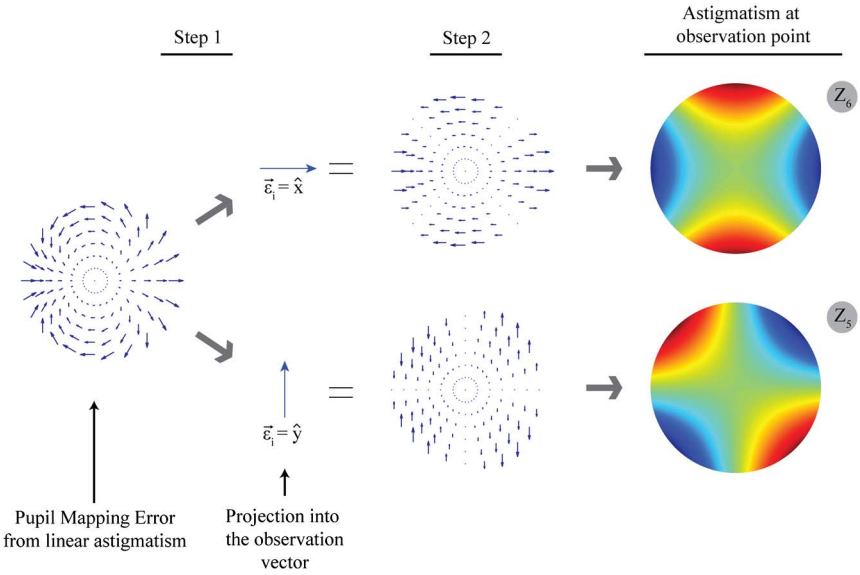

Fig. 6. (Color online) Illustration of Eq. (8). Step 1, quiver plot representation of the form of pupil mapping error from linear astigmatism. Step 2, projection of pupil mapping error onto the observation vectors and the resulting form of astigmatisms.

exit pupils, and then the departure from the ideal pupil mapping will be used to quantify the alignment of the optical system. Thus, the test needs to measure the mapping between angles θ_o and θ_i in Fig. 1. This is achieved by converting angular mapping to spatial mapping.

The angle θ_o can be defined by placing a test target consisting of an array of dots in the EP. An analyzer target would then be placed at the XP and would consist of an array of cross hairs. The cross hairs and the imaging point I would then be used to define θ_i, and the pupil mapping could be found. However, the EP and XP are not always at convenient locations to place targets, nor is it necessary to place the targets at the EP and XP. As long as θ_o and θ_i are defined in the object and image space, the targets do not have to be at the EP and XP. The setup in Fig. 7 shows a point source and test target in object space, which are used to define θ_o entering the EP. The image of the point source and an analyzer target define θ_i exiting the exit pupil, and the pupil mapping can be determined using Eq. (8). The analyzer target does not need to be at a conjugate image location to the test target. However, if the analyzer is not conjugate to the test grating, the image of the test target at the analyzer would be defocused, which could increase the uncertainty in the measurement of θ_i, increasing the uncertainty in the pupil mapping measurement.

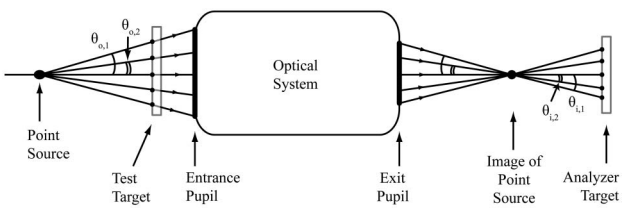

Fig. 7. Sketch of the general measurement approach to convert the angular mapping of θ_o and θ_i into a spatial mapping.

Also, it is important to note that when the test target consists of an array of dots, the accuracy of the test is dependent on the placement of the point source and two targets, as well as the placement of the points on the test and analyzer targets. For example, if the point source is not in the correct location with respect to the optical system, different aberrations will be found in the pupil mapping than would be expected from the optical design.

The mapping can also be measured easily and to high accuracy by using gratings as the two patterns and using the moiré effect created when the test grating is imaged onto the analyzer grating to measure the deviation of the pupil mapping. Additionally, when the test grating is illuminated by a point source, multiple orders of light are diffracted. In the next section, we will discuss how additional information can be gathered when different orders are selectively interfered.

5. Alternative, Wave Optics Explanation

In previous sections we have explained the SCTest from a geometrical optics perspective. In this section, we will expand on the idea of implementing the SCTest with gratings by explaining the test in terms of wave optics. By explaining the SCTest using wave optics, we highlight the fact that while the SCTest uses test components positioned on-axis, it measures the off-axis performance. In Fig. 8 the light from the point source illuminates the test grating and is diffracted into different orders, which are used to measure the off-axis performance where each order corresponds to a measurement at a different point in the field. For this explanation only the ± 1 orders are shown. As the ± 1 orders travel through the optical system under test, each beam is aberrated by the section of the optical system that it passes through. The behavior of the ± 1 orders is analogous

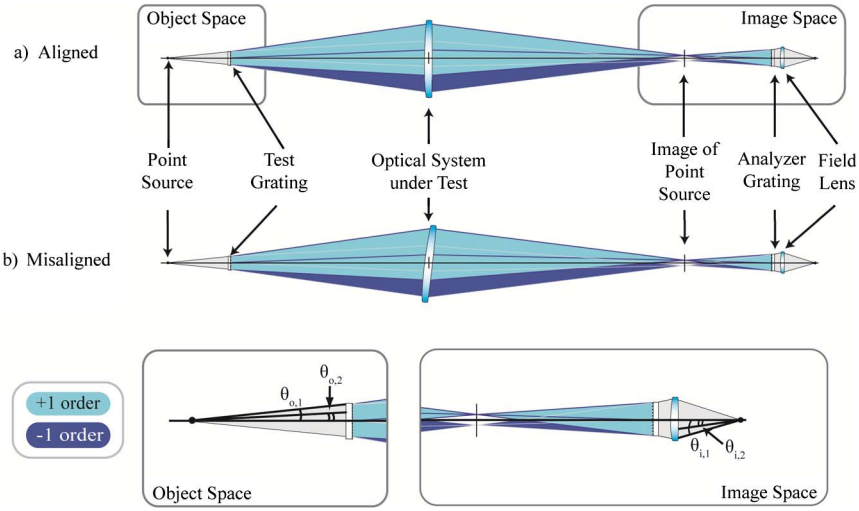

Fig. 8. (Color online) Diagram of the alternative measurement explanation, which uses a grating to create two beams that act as the two test beams used in interferometry. (a) The optical system under the test axis is aligned to the point source and test grating. (b) The optical system under test is tilted with respect to the point source and test grating Close-up of object space showing θ_o from Fig. 7 (object space inset) and close-up of image space showing θ_i from Fig. 7 (image space inset).

to the two beams of an interferometer. The analyzer then diffracts one order from both of the +1 and −1 orders back along the axis. When these wavefronts interfere, they produce a fringe pattern that shows the difference between the two orders. Again, this is similar to the resulting interferogram from an interferometer. In order to image this interferogram, a second aperture that only passes the orders from the analyzer that are along the optical axis is placed before the camera. This aperture is not shown in Fig. 8. See Fig. 9 in Section 6 for details of the experimental setup.

For the aberrations that have linear field dependence such as coma, the amount of aberrations added to the two beams shown in Fig. 8(a) is equal and opposite, so when the two beams interfere at the analyzer, the linear aberrations add. For aberrations with quadratic field dependence, such as astigmatism, the amount of aberration that the two beams acquire is equal and cancels in the interference pattern. However, when the optical system under test is tilted with respect to the point source and test grating, as shown in Fig. 8(b), the amount of astigmatism in the two beams is no longer equal. This results in residual astigmatism in the interferogram, where the amount of residual astigmatism increases linearly with field. Decentering the optical system under test would also result in linear astigmatism.

The amount of coma, however, in the interferogram does not change with the misalignment of the optical system. This can cause practical problems when analyzing the amount of aberrations in the interferogram. Because the SCTest can be used to measure systems that do not meet the sine condition, the optical system may have a nonnegligible amount of coma. When this happens, it is difficult to measure a small amount of astigmatism in the presence of a large amount of coma. To counteract this, one of the gratings can be fabricated as a computer-generated hologram (CGH). The CGH would both diffract the light from the point source and add coma to one of the sets of orders that is opposite to the amount that would be acquired as the beams propagate.

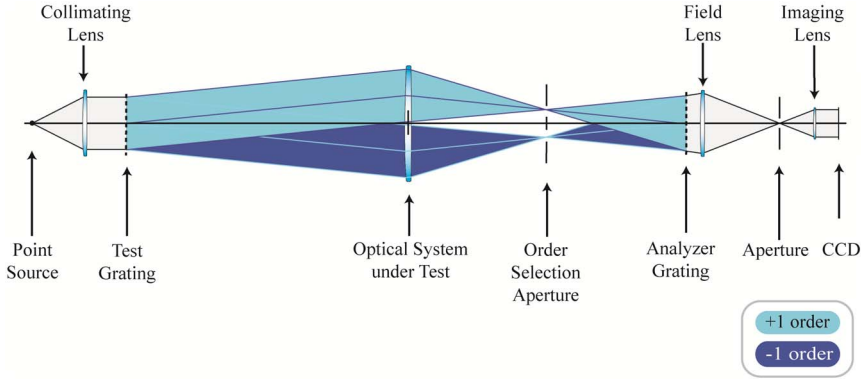

Fig. 9. (Color online) Illustration of the SCTest experimental setup on a single lens as well as the layout of the ZEMAX model of the experimental system.

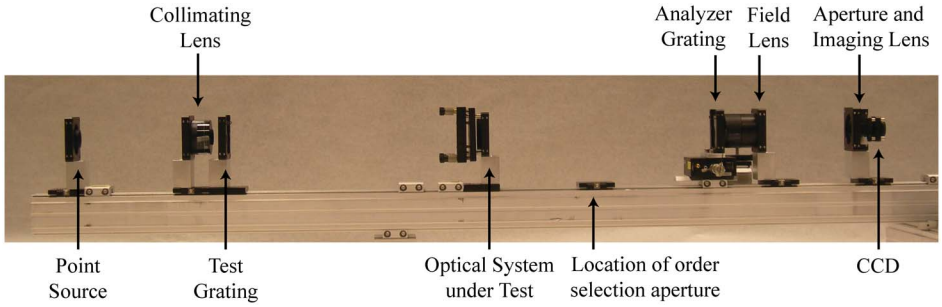

Fig. 10. (Color online) Picture of experimental system illustrated in Fig. 9. The order selection aperture is not pictured.

6. Experimental Results

This section explains the implementation of the SCTest on a physical system. Figure 9 is an illustration of the test on a single lens with the following components. Additionally, Fig. 10 shows a picture of the experimental setup.

1. Point source and collimating lens—the point source is the reference point for the test. The collimating lens collimates the light, placing the reference point at infinity ($\lambda = 632.8\,\text{nm}$).
2. Test grating—the test grating diffracts the beam into different orders. For this test, a Ronchi ruling with 10 lp/mm was used.
3. Optical system under test—a doublet (focal length = 200 mm) was used as the optical system under test, which focuses the collimated beams to an intermediate image plane at the order selection aperture. The doublet also images the test grating onto the analyzer grating.
4. Order selection aperture—this aperture selects the orders that will be interfered.
5. Analyzer grating—this grating diffracts the selected orders back along the optical axis. A Ronchi ruling with 10 lp/mm was also used for this grating. Either the analyzer grating or the test grating can be moved for phase shifting.
6. Field lens, second aperture plane, image lens, and CCD—these elements image the analyzer onto the CCD. The second aperture plane only passes the orders that were diffracted back along the optical axis by the analyzer grating.

For this experiment, the order selection aperture was set so that only the first orders were passed. Next, the position of the analyzer grating was set to minimize tilt fringes in the interferogram. Last, the analyzer was translated to create a phase shift of the fringes. Five images were recorded with a 90° phase shift between them. The order selection aperture was then reset two more times to pass the third and then the fifth orders to measure the aberrations in those orders. Figure 11 shows one of the interference patterns for each of the sets of measurements. Note, each measurement is the difference of the wavefront from two points in the field. In order to measure the linear component of astigmatism, only one measurement is necessary. For this experiment, the first-order measurements were used to set the alignment of the optical elements in the ZEMAX model of the system, and the third- and fifth-order measurements were used to evaluate how well the model matched the experiment. Details of the model can be found later in this section.

In the data, there is an obvious increase in tilt fringes as the order of the interfered beams increases. For the first-order interferogram, the two lobes of coma without tilt can be seen, and for the third-order interferogram the S-shape of coma with tilt is visible. For the fifth-order interferogram, the fringes are curved, but the additional tilt fringes makes the coma less obvious. The additional tilt fringes are a byproduct of the distortion of the optical system under test. Specifically, the intermediate image height at the order selection aperture, the distance from the optical

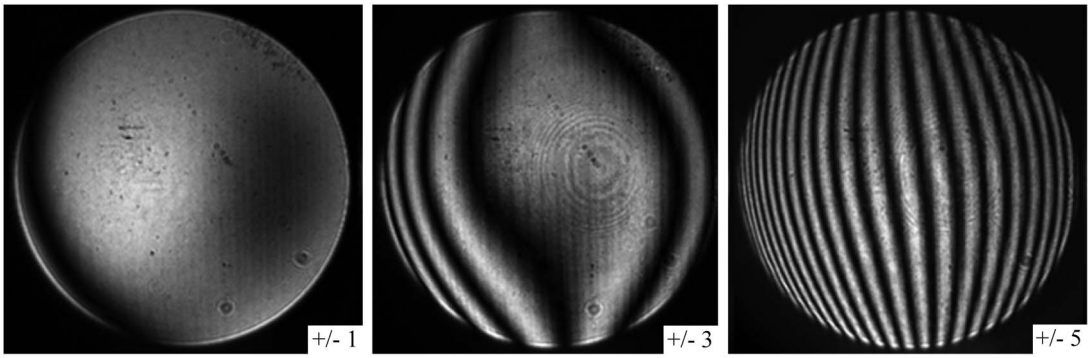

Fig. 11. Images of interferogram. Interference of (a) first orders, (b) third orders, (c) fifth orders.

Table 1. Measured and Predicted Data in Pairs of Orders as a Function of Zernike Standard Polynomials

Aberration	Orders	Measured (nm rms)	Predicted (nm rms)	Difference (nm rms)	Percent Error
Coma	first	0.120	0.114	0.006	4.7%
	third	0.360	0.340	0.020	5.5%
	fifth	0.669	0.554	0.115	17.2%
Astigmatism	first	0.066	used for fitting		
	third	0.194	0.202	−0.008	−3.9%
	fifth	0.355	0.348	0.007	1.9%
Power	first	−0.051	used for fitting		
	third	−0.150	−0.156	0.006	−3.9%
	fifth	−0.271	−0.269	−0.002	0.6%
Tilt	first	0.300	used for fitting		
	third	0.925	0.820	0.105	11.3%
	fifth	4.150	4.081	0.069	1.7%

system to the analyzer, and the frequency of the analyzer grating determine the diffracted angle of the light after the analyzer grating. If the lens has distortion, the intermediate image heights will not be ideal, which alters the diffracted angle of the light and causes tilt fringes in the interferogram. It is possible to set the spacing of the analyzer from the optical system such that the interferogram for a set of orders has no tilt fringes. However, the number of tilt fringes will be higher for the other orders.

To verify these results, the system layout shown in Fig. 9 was modeled in ZEMAX. To create a more complete model, the spherical aberration of the lens was measured and included. The optical system under test and the analyzer were then tilted independently in the model until the astigmatism and power for the first-order interferogram in the model matched the measured result. The spacing between the optical system under test and the analyzer in the model was also varied until the tilt of the first-order interferogram matched the measured results. In order to match the misalignments in the experimental system, the optical system under test and the analyzer were tilted in ZEMAX by 0.09° and 1.14°. The comparison between the measured and predicted results can be found in Table 1. No adjustments were made in the model to match the predicted coma values to the experimental coma values.

As can be seen from Table 1, the measured results match the predicted results well. Another thing to note is that in all of the measured data, the aberrations in the third-order beams are almost exactly three times the aberrations in the first-order beams. The aberrations in the fifth-order beams depart slightly from what one would expect if the field dependence were perfectly linear. Because there is small higher order dependence and higher order data is more likely to have noise, this error is not surprising. Also, it is worth explicitly stating that while the test optical system is a single lens, it is possible to have linear astigmatism if the axis of the beam entering the test grating is not coincident with the axis of the lens.

7. Conclusion

In this paper we have presented a description of the sine condition and how it can be used to find the pupil mapping to quantify system misalignment. To illustrate the implementation of this test, we provided an explanation in terms of geometric optics, as well as an explanation of the measurement in terms of wave optics. Finally, we presented results of our experimental system that match the model well.

References

1. E. Abbe, "Beitrage zur Theorie des Mikroskops und der mikroskopischen Wahrnehmung," Archiv Mikrosk. **9**, 413–418 (1873).
2. L. Mertz, "Geometrical design for aspheric reflecting systems," Appl. Opt. **18**, 4182–4186 (1979).
3. J. H. Burge and R. P. Angel, "Wide-field telescope using spherical mirrors," Proc. SPIE **5174**, 83–92 (2003).
4. R. Kingslake, *Lens Design Fundamentals*, 2nd ed. (Academic, 2010).
5. M. Shibuya, "Exact sine condition in the presence of spherical aberration," Appl. Opt. **31**, 2206–2210 (1992).
6. C. Zhao and J. H. Burge, "Criteria for correction of quadratic field-dependent aberrations," J. Opt. Soc. Am. A **19**, 2313–2321 (2002).
7. J. H. Burge, C. Zhao, and S. H. Lu, "Use of the Abbe sine condition to quantify alignment aberrations in optical imaging systems," Proc. SPIE **7652**, 765219 (2010).
8. B. McLeod, "Collimation of fast wide-field telescopes," Publ. Astron. Soc. Pac. **108**, 217–219 (1996).
9. L. Noethe, "Final alignment of the VLT," Proc. SPIE **4003**, 382–390 (2000).
10. H. Lee, "Optimal collimation of misaligned optical systems by concentering primary field aberrations," Opt. Express **18**, 19249–19262 (2010).
11. R. Tessieres, *Analysis for Alignment of Optical Systems* (University of Arizona, 2003).
12. M. Born and E. Wolf, *Principles of Optics: Electromagnetic Theory of Propagation, Interference and Diffraction of Light*, 7th ed. (Cambridge University, 1999).
13. M. Mansuripur, *Classical Optics and Its Applications*, 1st ed. (Cambridge University, 2002).
14. R. K. Luneburg, *Mathematical Theory of Optics*, 1st ed. (University of California, 1964).
15. H. A. Buchdahl, *An Introduction to Hamiltonian Optics* (Cambridge University, 1970).
16. R. V. Shack and K. Thompson, "Influence of alignment errors of a telescope system on its aberration field," Proc. SPIE **251**, 146–151 (1980).
17. P. L. Schechter and R. S. Levinson, "Generic misalignment aberration patterns in wide-field telescopes," Publ. Astron. Soc. Pac. **123**, 812–832 (2011).
18. T. Schmid, K. P. Thompson, and J. P. Rolland, "Misalignment-induced nodal aberration fields in two-mirror astronomical telescopes," Appl. Opt. **49**, D131–D144 (2010).